

# Effect of Magnetization Inhomogeneity on Magnetic Microtraps for Atoms

S. W. Hiltz, B. V. Hall, T. Roach, R. Anderson, P. Hannaford, and A. I. Sidorov  
 ARC Centre of Excellence for Quantum Atom Optics and  
 Centre for Atom Optics and Ultrafast Spectroscopy,  
 Swinburne University of Technology, Hawthorn, Victoria 3122, Australia  
 (Dated: April 23, 2019)

We report on the origin of fragmentation of ultracold atoms observed on a permanent magnet in atom chip. A novel technique is used to characterize small spatial variations of the magnetic field near the in surface using radio frequency spectroscopy of the trapped atoms. Direct observations indicate the fragmentation is due to a corrugation of the magnetic potential caused by long range inhomogeneity in the in magnetization. A model which takes into account two-dimensional variations of the in magnetization is consistent with the observations.

PACS numbers: 03.75.Be, 07.55.Ge, 34.50.Dy, 39.25.+k

An atom chip is designed to manipulate magnetically trapped ultracold atoms near a surface using an arrangement of microfabricated wires or patterned magnetic materials [1]. Since the realization of Bose-Einstein condensates (BECs) on atom chips [2, 3], pioneering experiments have studied single-mode propagation along waveguides [4], transport and adiabatic splitting of a BEC [5] and recently on-chip atom interferometry [6, 7]. Permanent magnets are particularly attractive for atom chips as they can provide complex magnetic potentials while suppressing current noise that causes heating and limits the lifetime of trapped atoms near a surface [8]. To date, permanent magnet atom chips have been developed with a view to study one-dimensional quantum gases [9, 10], decoherence of BEC near surfaces [8, 11], hybrid magnetic and optical trapping configurations [12], and self-biased all-magnetic potentials [13]. It has been found, however, that in addition to current noise, atom chips have other limitations, as undesired spatial magnetic field variations associated with the current-carrying wires or magnetic materials act to fragment the trapped atoms.

In previous work, fragmentation of atoms trapped near current-carrying wires was traced to roughness of the wire edges that causes tiny current deviations [14, 15]. This introduces a spatially varying magnetic field component parallel to the wire which corrugates the bottom of the trap potential. While more advanced microfabrication techniques have been used to produce wires with extremely straight edges, thereby minimizing fragmentation [16], the first experiments with permanent magnet atom chips have now also indicated the presence of significant fragmentation [17, 18]. This has motivated further work towards understanding the mechanisms that cause fragmentation near magnetic materials.

In this Letter we report on the origin of fragmentation near the surface of a permanent magnet in atom chip. To characterize the magnetic field near the in surface we have developed a new technique which combines precision radio frequency (RF) spectroscopy of trapped atoms with high spatial resolution. This allows sensitive and in-

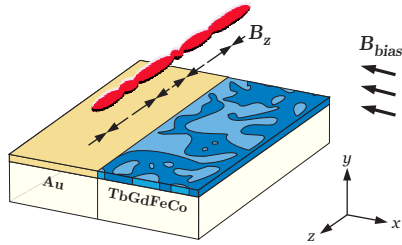


FIG. 1: (Color online) Schematic diagram of a permanent magnet in atom chip. Inhomogeneity in the in magnetization leads to fragmentation of the trapped cloud of ultracold atoms when positioned near the surface.

trinsically calibrated measurements of the magnetic field landscape to be made over a large area. We find the fragmentation originates from long range inhomogeneity in the in magnetization and has characteristics that differ from those observed for current-carrying wire atom chips. To account for the observations we have developed a model for the spatial decay of random magnetic fields from the surface due to inhomogeneity in the in magnetization.

A schematic diagram of a basic permanent magnet in atom chip is shown in Fig. 1. Our atom chip consists of a  $Tb_6Gd_{10}Fe_{80}Co_4$  in on a  $300\text{ }\mu\text{m}$  thick glass-slide substrate [11]. The edge of the substrate is polished to optical quality prior to in deposition. Scanning probe measurements on similarly prepared substrates indicate that the residual edge roughness is less than  $50\text{ nm}$  and the top surface is extremely smooth. The substrate is sputter-coated with a multilayer magneto-optical in ( $6\text{--}150\text{ nm}$  TbGdFeCo and  $6\text{--}140\text{ nm}$  Cr) and a gold overlayer ( $100\text{ nm}$ ), and the in topology accurately follows that of the polished substrate. The deposited in has been analyzed using a SQUID magnetometer and a magnetic force microscope (MFM) and has excellent magnetic properties [19]. The in is then magnetized perpendicular to the surface by a magnetic field of  $1\text{ T}$  and afterwards is magnetically homogeneous

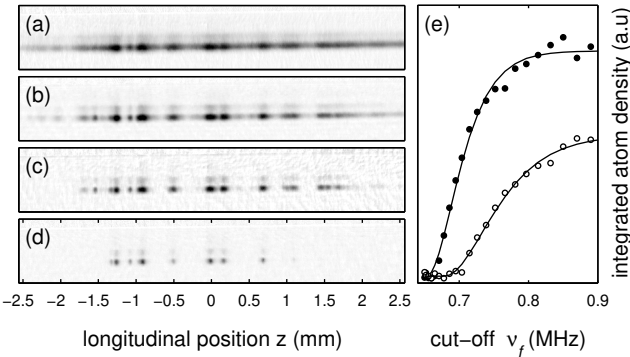


FIG. 2: Absorption images of the atomic density in the magnetic microtrap located  $y_0 = 67$   $\mu\text{m}$  from the surface. As the RF cut-off  $v_f$  is decreased, the structure of the potential is revealed. (a)  $v_f = 1238$  kHz, (b)  $v_f = 890$  kHz, (c)  $v_f = 766$  kHz, (d)  $v_f = 695$  kHz and (e) integrated atom density vs.  $v_f$  for two longitudinal positions,  $z = 0.69$  mm (solid circles) and  $z = 1.00$  mm (open circles), fitted to the truncated thermal distribution function (Eq. 1).

within the sensitivity of the MFM. A second glass slide, coated with a non-magnetic gold film, completes the reflective atom chip surface (Fig. 1). Both substrates are then epoxied to a 500  $\mu\text{m}$  thick silver foil current-carrying structure which is used for loading ultracold atoms into the permanent magnet microtrap, to provide weak longitudinal confinement, and as an in-built radio frequency antenna.

At the edge of the perpendicularly magnetized film a field is produced that is analogous to that of a thin current-carrying wire aligned with the film edge ( $I_{\text{eff}} = 0.2$  A) [11]. A magnetic microtrap is formed by the field from the film, a uniform magnetic field  $B_{\text{bias}}$ , and two current-carrying end wires. In the experiment  $2 \times 10^8$   $^{87}\text{Rb}$  atoms are collected in a mirror magneto-optical trap located 5 mm from the surface. These atoms are optically pumped to the  $F = 2, m_F = +2$  hyperfine state and subsequently transferred to a magnetic trap formed by a Z-shaped current-carrying wire and  $B_{\text{bias}}$ . A preliminary RF evaporative cooling stage is used to reduce the cloud temperature below 5  $\mu\text{K}$ . The remaining atoms are then transferred to the magnetic microtrap by adiabatically reducing the current through the Z-shaped wire to zero. The final values of  $B_{\text{bias}}$  vary from 0.2 mT to 0.8 mT, so the transverse trap frequency varies between 2–410 Hz and 2–1500 Hz while the trap position  $y_0$  ranges from 200  $\mu\text{m}$  to 50  $\mu\text{m}$  from the surface. The end-wires are operated at 0.5 A such that the trap depth is 100  $\mu\text{K}$  and the elongated cloud of atoms extends across 5 mm of the atom chip surface to allow measurement of the magnetic potential.

The narrow energy distribution of ultracold atoms is an inherent advantage when used as a probe of weak potentials. In particular, the equilibrium distribution of trapped atoms has been used to image magnetic fields

near test wires with high sensitivity and high spatial resolution [20, 21]. In parallel, RF spectroscopy has been used as a precise and powerful method for investigating the properties of cold atom clouds [22, 23, 24, 25, 26]. In this paper we describe a new technique using RF spectroscopy of ultracold atoms to accurately probe small magnetic field variations near the magnetic film surface.

A spatially uniform RF field of frequency  $\omega$  is applied perpendicular to the trap axis to resonantly outcouple atoms to untrapped magnetic states at positions where  $g_F B \beta(x; y; z) = \hbar \omega$ . The RF field is swept using a single frequency ramp (0.2 MHz/s) from 2 MHz to a final cut-off frequency  $v_f$  ranging between 1.4 MHz and 0.5 MHz. The Rabi frequency of the RF transition is 2–0.5 kHz, high enough to ensure that atoms with total energy greater than  $\hbar \omega$  are removed from the trap with high probability and that regions of the potential where  $g_F B \beta(x; y; z) > \hbar \omega$  thereafter remain unpopulated. During the early stages of the RF sweep the cloud undergoes some evaporative cooling as the in-trap collision rate is high enough to allow rethermalization. At the end of the sweep the resonant frequency approaches that corresponding to the trap bottom and the cloud becomes significantly truncated by the RF field.

Immediately after the sweep,  $B_{\text{bias}}$  is switched off to accelerate the atoms away from the film surface in the remaining permanent magnetic field gradient. The longitudinal density distribution is unperturbed during the 1 ms expansion time and is an accurate representation of the in-trap distribution. A resonant absorption image is then recorded by a CCD with a spatial resolution of 5  $\mu\text{m}$ . A series of absorption images for different values of  $v_f$  is shown in Fig. 2. Noticeable fragmentation is observed when  $v_f$  is reduced below 1.3 MHz (Fig. 2a). For  $v_f < 0.9$  MHz the density distribution becomes truncated by the RF field and regions of the atomic density decrease to zero (Fig. 2b). Reducing  $v_f$  further results in well separated clumps of atoms which are found only in the lowest potential wells (Fig. 2c, d).

For a quantitative analysis we assume that the full trapping potential can be expressed in terms of the transverse confinement and the corrugated longitudinal potential  $m_F B \beta_z(z)$  [15]. The atomic distribution in the trap immediately after the RF sweep is described by a truncated Boltzmann distribution [23, 27]. To extract  $\beta_z(z)$ , the integrated atom density as a function of  $v_f$  is fitted for each position  $z$  to the truncated thermal distribution function (Fig. 2e),

$$n(z; v_f) = n_1(z) \left[ \text{erf} \left( \frac{p}{2} \right) - \frac{p}{2} \right] = e^{-\left( \frac{p}{2} \right)^2} \left[ 1 - \text{erf} \left( \frac{p}{2} \right) \right], \quad (1)$$

where  $n_1$  is the integrated atom density before truncation and the spatially dependent truncation parameter is

$$(z; v_f) = (\hbar \omega_f - g_F B \beta_z(z)) / k_B T; \quad (2)$$

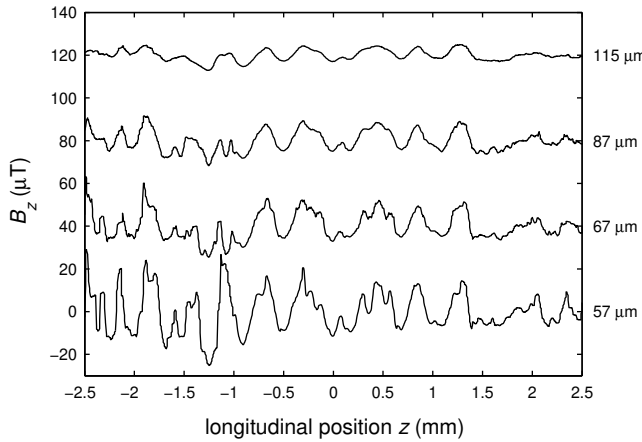


FIG. 3: Magnetic field profiles measured using spatially resolved RF spectroscopy for various distances to the surface. The effect of weak longitudinal confinement is subtracted and each profile has been offset by 40  $\mu\text{T}$  for clarity.

where  $T$  is a fit parameter, which characterizes the non-equilibrium distribution during truncation. We note that this model does not appropriately describe regions of the potential where the atomic density is large, such as the bottom of the potential wells. To extract the magnetic potential in these areas we fit Eq. 1 over values of  $\epsilon$  that excludes high atomic density. After reconstructing the magnetic field profile the effect of the end-wires is subtracted. The statistical uncertainty in the measurement is approximately 0.1  $\mu\text{T}$ , which is mainly attributed to fluctuations of external magnetic fields. With appropriate magnetic shielding the expected sensitivity of the technique is limited by the power broadened RF linewidth required to effectively outcouple atoms.

Complete magnetic field profiles are given for several distances from the In in Fig. 3. Firstly, the amplitude and structure of the corrugated potential are constant from day to day; however the amplitude increases as the trap is positioned closer to the surface, with an approximate power law dependence given by  $y^a$ , where  $a = 1.8 - 0.3$ . For  $y_0 > 100 \mu\text{m}$  the potential has a characteristic period of about 390  $\mu\text{m}$ , significantly longer than that commonly observed near electroplated wires [15, 28]. Closer to the In, additional corrugations appear with a characteristic period of about 170  $\mu\text{m}$ . These y-dependent characteristics of the potential have allowed time-dependent manipulation of BECs at particular interesting regions of the disordered potential [18].

We have found that the amplitude of the corrugated potential is not consistent with magnetostatic calculations based on fluctuations of the In edge (Fig. 4), suggesting that the cause of fragmentation may be spatial variations of the magnetization within the body of the In. To investigate this, a second bias field is applied in the y direction to bring the trap closer to the

surface while keeping a constant distance from the edge of the magnetic In. A cloud of atoms positioned 50  $\mu\text{m}$  from the surface of the magnetic In and 100  $\mu\text{m}$  from the edge is significantly fragmented, while a cloud positioned 50  $\mu\text{m}$  above the non-magnetic gold In does not exhibit atomic density variations. This observation confirms that the magnetic field variations originate from the magnetic material itself and not from imperfections along the edge of the In.

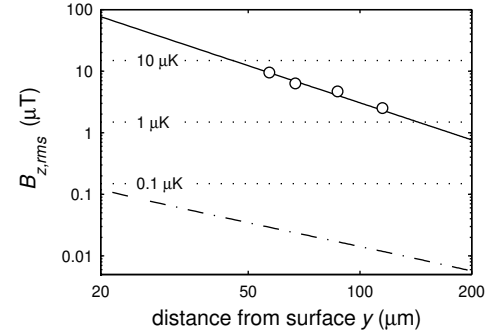


FIG. 4: Behavior of the magnetic field roughness as a function of distance from the In surface. The dashed line corresponds to the situation of a homogeneous In with a fluctuating edge as measured by a profilometer. The solid line is a fit to the data using Eq. 4 which corresponds to white noise magnetization variations within the body of the In with a characteristic feature size  $d = 5 \mu\text{m}$  and  $M = M_s / 0.4$ .

Our model describes the effect of two-dimensional spatial variations in the perpendicular magnetization  $M_y(x; z)$  of the In. Inhomogeneity leads to the appearance of a random magnetic field above the surface, of which, we are most interested in the magnetic field component  $B_z(x; y; z)$  that corrugates the bottom of the trapping potential. Using a standard approach incorporating the two-dimensional Fourier transform of the random magnetization  $N(k_x; k_z)$  and the magnetic scalar potential we obtain an expression for the  $B_z$  component of the corrugated magnetic field. In the case of a magnetic In occupying a half-plane with the edge at  $x = 0$  (Fig. 1) and arbitrary magnetization noise we have, for heights greater than the In thickness,

$$B_z = i2 \int_0^y dk_x dk_z k_z^2 N(k_x; k_z) e^{i2(k_x x + k_z z)} \int_x^1 \int_{k_z=1}^1 \frac{p}{dx} e^{i2(k_x x + k_z z)} \frac{K_1(2k_z \sqrt{\frac{p}{x} \frac{x^2 + y^2}})}{\sqrt{\frac{p}{x} \frac{x^2 + y^2}}}; \quad (3)$$

where  $p$  is the In thickness and  $K_1$  is the modified Bessel function of the second kind. In general this expression can be used to describe any planar pattern of elements that can be represented as a linear combination of step functions.

In the case of white noise fluctuations in the magnetization,  $N(k_x; k_z) = \text{const}$ , the rms value of the mag-

netic field roughness can be evaluated analytically. We perform ensemble averaging and find

$$B_{z;\text{rms}} = \frac{r}{\sqrt{\frac{3}{16} d M}} \sqrt{1 + \frac{15}{8} \left(\frac{5}{4}\right)^3 + \frac{3}{8} \left(\frac{5}{4}\right)^5}; \quad (4)$$

where  $r = \sqrt{x^2 + y^2}$ ,  $M$  is the rms magnetization inhomogeneity and  $d$  is the characteristic feature size of the domain structure. For  $x = 0$  the model predicts that the corrugated magnetic field component decays with a  $y^2$  dependence, consistent with our experimental result. This behavior can also be compared with the more rapid decay ( $\propto y^{2.5}$ ) expected for white noise fluctuations of the edge of current-carrying wires [14, 15]. Film edge fluctuations are expected to produce corrugations three orders of magnitude smaller than that observed in the experiments (Fig. 4). The model also predicts the fast decay of the corrugated magnetic field away from the film edge for  $x < 0$ .

In Fig. 4 the experimental results are compared with the model with relevant energy scales indicated by dotted lines. The characteristic feature size and distribution function of the domain structure has been inferred from MFM measurements of a demagnetized TbGdFeCo film and is found to have close to white noise characteristics with  $d = 5 \mu\text{m}$ . The best fit of Eq. 4 to the data is found for  $M = M_s = 0.4$  where  $M_s$  is the saturation magnetization of the film. If the inhomogeneity is assumed to originate from reversal of a small number of magnetic domains ( $M_y(x; z) = M_s$ ) then we conclude that the mean magnetization of the film is  $0.9M_s$ .

The TbGdFeCo magnetic film was originally chosen for its desirable magnetic properties including a large coercivity ( $H_c = 0.32 \text{ T}$ ) and a high Curie temperature ( $T_c = 300 \text{ C}$ ) [19]. We attribute the observed inhomogeneity to deterioration of the magnetic film experienced during the vacuum bake-out (140 C over 4 days) despite the relatively high Curie temperature of our film. This conclusion is consistent with reports of reduced perpendicular anisotropy found for similar films after annealing at temperatures above 100 C [29, 30] and with our own measurements on similar films.

In conclusion, trapped ultracold atoms are extremely sensitive to small magnetic field variations found near the surface of a permanent magnetic film. These variations corrugate the longitudinal trapping potential and result in fragmentation of atomic density. We have developed the technique of spatially resolved RF spectroscopy as a powerful method for accurately mapping small magnetic field variations near the surface of the magnetic film. A simple model accounts for spatial inhomogeneity of the film magnetization and agrees well with the observations. The development of new permanent magnetic atom chips will require additional research aimed at further optimiz-

ing the quality of magnetic films.

We would like to thank J. Wang for the deposition of the magnetic film. This project is supported by the ARC Centre of Excellence for Quantum Atom Optics and a Swinburne University Strategic Initiative grant.

Electronic address: brhalla@swin.edu.au

- [1] R. Folman, P. K. ruger, J. Schmiedmayer, J. Denschlag, and C. Hensel, *Adv. At. Mol. Opt. Phys.* **48**, 263 (2002).
- [2] W. Hensel, P. Hommelhofer, T. W. Hansch, and J. Reichel, *Nature* (London) **413**, 498 (2001).
- [3] H. Ott, J. Fortagh, G. Schlotterbeck, A. Grossmann, and C. Ziemann, *Phys. Rev. Lett.* **87**, 230401 (2001).
- [4] A. E. Leanhardt et al., *Phys. Rev. Lett.* **89**, 040401 (2002).
- [5] P. Hommelhofer, W. Hensel, T. Steinmetz, T. W. Hansch, and J. Reichel, *New J. Phys.* **7**, 3 (2005).
- [6] Y. Shin et al., *Phys. Rev. A* **72**, 021604(R) (2005).
- [7] T. Schumm et al., *Nature* (London) **1**, 57 (2005).
- [8] C. D. J. Sinclair et al., *Phys. Rev. A* **72**, 031603(R) (2005).
- [9] M. Vengalattore, R. S. Conroy, W. Roodijkers, and M. Prentiss, *J. Appl. Phys.* **95**, 4404 (2004).
- [10] I. Llorente-Garcia et al., *J. Phys.: Conf. Ser.* **19**, 70 (2005).
- [11] B. V. Hall et al., *J. Phys. B: At. Mol. Opt. Phys.* **39**, 27 (2006).
- [12] A. Jaakkola et al., *Eur. Phys. J. D* **35**, 81 (2005).
- [13] I. Barb, R. Gerritsma, Y. T. Xing, J. B. Gaoedkoop, and R. J. C. Spreeuw, *Eur. Phys. J. D* **35**, 75 (2005).
- [14] D. W. Wang, M. D. Lukin, and E. Demler, *Phys. Rev. Lett.* **92**, 076802 (2004).
- [15] J. E. steve et al., *Phys. Rev. A* **70**, 043629 (2004).
- [16] P. K. ruger et al., cond-mat/0504686 (2004).
- [17] C. D. J. Sinclair et al., *Eur. Phys. J. D* **35**, 105 (2005).
- [18] B. V. Hall et al., in *Laser Spectroscopy XVII*, edited by E. A. Hinds, A. Ferguson, and E. R. Ries (World Scientific, Singapore, 2005).
- [19] J. Y. Wang et al., *J. Phys. D: Appl. Phys.* **38**, 4015 (2005).
- [20] S. W. ildemuth et al., *Nature* (London) **435**, 440 (2005).
- [21] A. G. unther et al., *Phys. Rev. A* **71**, 063619 (2005).
- [22] A. G. M. artin, K. Helmerson, V. S. Bagnato, G. P. Lafayatis, and D. E. Pritchard, *Phys. Rev. Lett.* **61**, 2431 (1988).
- [23] K. Helmerson, A. G. M. artin, and D. E. Pritchard, *J. Opt. Soc. Am. B* **9**, 483 (1992).
- [24] I. Bloch, T. W. Hansch, and T. Esslinger, *Phys. Rev. Lett.* **82**, 3008 (1999).
- [25] S. G. Gupta et al., *Science* **300**, 1723 (2003).
- [26] C. Chin et al., *Science* **305**, 1128 (2004).
- [27] O. J. Luiten, M. W. Reynolds, and J. T. M. W. alraven, *Phys. Rev. A* **53**, 381 (1996).
- [28] J. Fortagh, H. Ott, S. Kraft, A. G. unther, and C. Ziemann, *Phys. Rev. A* **66**, 041604(R) (2002).
- [29] F. E. Luborsky, *J. Appl. Phys.* **57**, 3592 (1985).
- [30] Y. J. Wang and Q. W. Leng, *Phys. Rev. B* **41**, 651 (1990).